IEEE Open Journal of Vehicular Technology

Received 29 October 2024; accepted 27 November 2024. Date of publication 2 December 2024;
date of current version 17 December 2024. The review of this article was coordinated by Editor Evgenii Vinogradov.

Digital Object Identifier 10.1109/OJVT.2024.3509646

Optimal Linear Precoding Under Realistic Satellite Communications Scenarios

GEOFFREY EAPPEN [1] (Member, IEEE), JORGE LUIS GONZALEZ [1] (Member, IEEE), VIBHUM SINGH [1] (Member, IEEE), RAKESH PALISETTY [2] (Member, IEEE), ALIREZA HAQIQTNEJAD [3] (Member, IEEE), LIZ MARTINEZ MARRERO [1] (Member, IEEE), JEVGENIJ KRIVOCHIZA [4] (Member, IEEE), JORGE QUEROL [1] (Member, IEEE), NICOLA MATURO [5] (Member, IEEE), JUAN CARLOS MERLANO DUNCAN [1] (Senior Member, IEEE), EVA LAGUNAS [1] (Senior Member, IEEE), STEFANO ANDRENACCI [4], AND SYMEON CHATZINOTAS [1] (Fellow, IEEE)

[1]Interdisciplinary Centre for Security Reliability and Trust, University of Luxembourg, 1855 Esch-sur-Alzette, Luxembourg
[2]Department of Electrical Engineering, Shiv Nadar Institution of Eminence Deemed to be University, Delhi 201314, India
[3]OQ Technology, 3364 Leudelange, Luxembourg
[4]SES S.A. Château de Betzdorf, L-6815 Betzdorf, Luxembourg
[5]European space Agency-ESA, 2201 AZ Leiden, Netherlands

CORRESPONDING AUTHOR: VIBHUM SINGH (e-mail: vibhum.singh@uni.lu).

This work was supported in part by the European Space Agency under Grant 4000122451/18/NL/NR and in part by the Luxembourg National Research Fund (FNR), through the CORE Project (ARMMONY): "Ground-based distributed beamforming harmonization for the integration of satellite and Terrestrial networks", under Grant FNR16352790.

ABSTRACT In this paper, optimal linear precoding for the multibeam geostationary earth orbit (GEO) satellite with the multi-user (MU) multiple-input-multiple-output (MIMO) downlink scenario is addressed. Multiple-user interference is one of the major issues faced by the satellites serving the multiple users operating at the common time-frequency resource block in the downlink channel. To mitigate this issue, the optimal linear precoders are implemented at the gateways (GWs). The precoding computation is performed by utilizing the channel state information obtained at user terminals (UTs). The optimal linear precoders are derived considering beamformer update and power control with an iterative per-antenna power optimization algorithm with a limited required number of iterations. The efficacy of the proposed algorithm is validated using the In-Lab experiment for 16 × 16 precoding with multi-beam satellite for transmitting and receiving the precoded data with digital video broadcasting satellite-second generation extension (DVB-S2X) standard for the GW and the UTs. The software defined radio platforms are employed for emulating the GWs, UTs, and satellite links. The validation is supported by comparing the proposed optimal linear precoder with full frequency reuse (FFR), and minimum mean square error (MMSE) schemes. The experimental results demonstrate that with the optimal linear precoders it is possible to successfully cancel the inter-user interference in the simulated satellite FFR link. Thus, optimal linear precoding brings gains in terms of enhanced signal-to-noise-and-interference ratio, and increased system throughput and spectral efficiency.

INDEX TERMS FFR, MU-MIMO, precoding, power control, satellite communications.

I. INTRODUCTION

During last decades, the multiple-input-multiple-output (MIMO) communications concept has had a surge in popularity in academia and industry. The MIMO concept, and in particular the massive-MIMO (M-MIMO) concept has been the most salient characteristic of the latest wireless communication standards including the fifth-generation (5G) of mobile radio systems, Wi-Fi, and even power line communications. However, this strong impulse has not been seen yet in the field of satellite communications (SATCOMs). To meet the high user demands, most SATCOM services focus on high throughput satellites (HTSs) with multiple spot

beams for enhancing spectral efficiency (SE) and high data rate connectivity. Primarily, in the multiple spot beams, full frequency reuse (FFR) is employed, leading to high SE [1]. The major challenge associated with the multiple spot beam is the interference between the adjacent beams owing to the presence of the side lobes in the beam radiation pattern on a particular coverage area [2].

Recent years have witnessed a strong impulse in adopting M-MIMO in wireless networks [3], [4]. Despite the wide literature related to M-MIMO for terrestrial networks, much less attention has been devoted to its possible exploitation in the forward link of SATCOM systems. As such, the 5G mobile radio communication systems aim to deliver seamless integration and enhanced flexibility across various telecommunication networks. Traditionally, terrestrial and satellite systems have developed separately, leading to significant technological differences between these networks. However, the vision of 5G heterogeneous networks includes SATCOM to increase the capacity of 5G networks in terms of better coverage, reliability, availability, and scalability. The coexistence of satellites and the 5G networks require interference-free links. The role of precoding schemes and power allocation is critical in guaranteeing interference-free communication with enhanced quality. Therefore, it is important to define standards for incorporating 5G with SATCOM. The 5GPPP research initiative, co-funded by the European Commission, aims to establish new unified standards for 5G networks [3]. Within this initiative, the METIS 2020 project focuses on laying the groundwork for next-generation mobile and wireless communication systems, targeting 2020 and beyond [4]. These standards will enable the seamless integration of mobile cellular communications and satellite systems into a unified service.

Incorporating modern SATCOM systems into 5G networks offers various use cases, such as extending coverage for traditional terrestrial cells, enabling caching through multicast/broadcast data transmission, and providing off-load backhauling for unicast user traffic [5], [6]. The digital video broadcasting satellite-second generation extension (DVB-S2X) [7] was developed to complement new scenarios for flexible SATCOM integration into 5G and beyond networks. MIMO precoding techniques are based on the closed-loop approach by employing the retrieved channel state information (CSI) from the user terminals (UTs), requiring a feedback channel from UT back to the gateway (GW). Due to the time-varying channel, the GW has only access to a delayed version of CSI, which can eventually limit the overall system performance [8], [9], [10], [11]. However, in contrast to general multiuser (MU) MIMO terrestrial systems, the CSI degradation in multibeam mobile applications has a very limited impact on typical fading channel and system assumptions. Under realistic conditions, the numerical results of [9] demonstrate that precoding can offer an attractive gain in the system throughput compared with the conservative frequency reuse (FR) allocations. Fig. 1 depicts the four-color FR scheme. MIMO precoding techniques, which are generally defined as

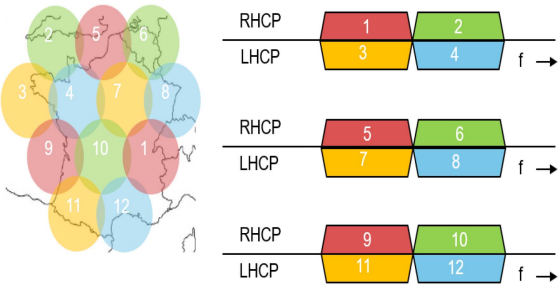

FIGURE 1. Four-color FR (4FR).

closed-form methods or approximate methods, are very quick and less complex. But, these methods provide suboptimal solutions and have to be solved by time-consuming iterative convex optimization (CVX) or non-negative least squares (NNLS) solving methods that must fit into a relevant time frame [12]. Recent research is advanced on the reduction of the processing times to meet channel requirements [11], [13].

Academic research shows that precoding techniques in SATCOM potentially allow more efficient spectral utilization and substantially higher service availability than the conservative four-color FR allocation for interference minimization [14], [15], [16], [17], [18], [19]. Zero-forcing (ZF) precoding was practically demonstrated in [20], [21], [22] using real-time signal processing and transmission.

To enable the efficient utilization of satellite transponders, multiple carriers have to be relayed through a single high power amplifier (HPA). However, the non-linear nature of the HPA results in adjacent channel interference and increased peak-to-average power ratio (PAPR), which limits the expected performance gains [23]. The symbol-level precoding design proposed in [24] allows controlling the instantaneous per-antenna transmit power, thus, leading to a reduction of the power peaks, which are detrimental to the aforementioned non-linearity problem. It should be mentioned that this is not possible in the channel-level approach, where the precoder is designed for an entire codeword, including several symbols. Hence, the transmitted power can be controlled only on an average basis, not on a symbol-by-symbol basis. In the context of nonlinear channels, it is also worth mentioning that more advanced symbol level precoding schemes [24], [25], [26], [27] which aim at reducing the PAPR of the transmitted waveform, considerably improve their robustness.

Inspired by the aforementioned discussion, in this paper, we consider an optimal minimum mean square error (MMSE) precoding scheme while employing a proper iterative per-antenna power optimization algorithm with a limited required number of iterations. This paper advances the field by designing, implementing, and experimentally evaluating the performance of MMSE algorithms with per-antenna optimization using a software-defined radio, specifically the universal software radio peripheral (USRP) platform. The study involves constructing a practical communication system, which includes a transmitter, a channel emulator, and a receiver.

Our work emphasizes on a multi-beam DVB-S2X compliant GW, incorporating a satellite MIMO channel emulator and considering the characteristics of UTs. In contrast to the method proposed in [6], which involves a two-step optimization process comprising beamformer updates and power control updates, we present an efficient iterative per-antenna power optimization algorithm. This proposed algorithm is specifically designed for satellite communication applications, offering rapid convergence within a limited number of iterations. This ensures computational efficiency and makes it particularly suitable for the complex nature of satellite communication systems.

In particular, we focus on creating a hardware demonstrator for a closed-loop 16 × 16 precoded SATCOM system. We develop the multi-beam DVB-S2X compliant GW, the satellite MIMO channel emulator, and the associated UTs. Further, we validate the design requirements with appropriate software and hardware resources. Notably, the DVB-S2X physical layer is implemented using commercial SDR platforms. The data interface for this DVB-S2X gateway adheres to the "Mode Adaptation input interface," delivering complete bundled frame packets alongside the corresponding MODCOD configuration [28]. All functional components of the DVB-S2X GW—such as scrambling, encoding, framing, modulation, and pulse-shaping—along with the precoding algorithm operate in real-time on the SDR. Utilizing SDR technology allows for rapid prototyping and deployment of the precoded transmission via the optimal MMSE precoding scheme in a realistic setting, as opposed to relying solely on numerical simulations. In summary, our main contributions in this paper can be pointed out as follows:

- We explore an optimal MMSE precoding scheme integrated with an efficient iterative per-antenna power optimization algorithm. This algorithm is designed to converge within a limited number of iterations, ensuring computational efficiency.
- The performance of the MMSE precoding scheme combined with per-antenna optimization algorithms is further experimentally evaluated using a Software-Defined Radio (SDR) platform, specifically the USRP.
- To assess the practical performance of our proposed solutions, we develop a comprehensive communication system. This includes a transmitter, a channel emulator, and a receiver, providing a realistic environment for testing.
- A hardware demonstrator for a closed-loop 16 × 16 precoded satellite SATCOM system is implemented, detailing the design and functionality of a multi-beam DVB-S2X compliant gateway, a satellite MIMO channel emulator, and a set of UTs.
- The system design requirements are validated using practical software and hardware resources. This includes demonstrating the real-time execution of DVB-S2X physical layer components such as scrambling, encoding, framing, modulation, and pulse-shaping, all implemented using SDR techniques.

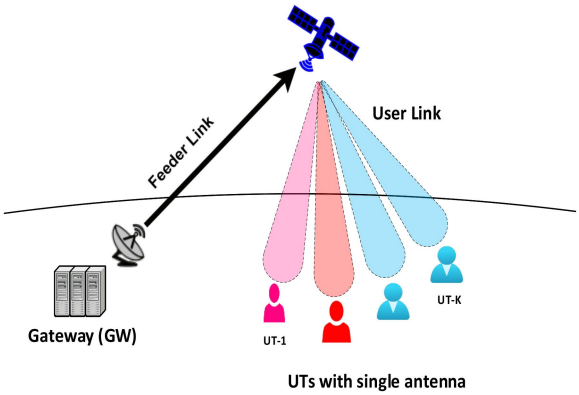

FIGURE 2. System model concept diagram.

- We utilize the "Mode Adaptation input interface" for the data format of the DVB-S2X gateway, guaranteeing that complete bundled frame packets are delivered along with the appropriate MODCOD configuration.
- By leveraging SDR technology, we achieve rapid deployment of the prototype, enabling us to test the optimal MMSE precoding scheme in a realistic environment, moving beyond mere numerical simulations.

The rest of this paper is organized as follows. In Section II, we describe the system model. Precoding implementation is presented in Section III. Section IV provides details on the experimental validation of the proposed methods, followed by concluding remarks in Section VI.

Notations: The upper-case and lower-case bold-faced letters are used to denote matrices and column vectors, respectively. The superscripts $(\cdot)^{\mathrm{H}}$, $(\cdot)^{\dagger}$, and $(\cdot)^{-1}$ represent the Hermitian, transpose, and inverse operations in the matrix, respectively. Further, $||\cdot||$ denotes an absolute magnitude of a complex value, whereas $\mathbf{I}$ being the Identity matrix.

II. SYSTEM DESCRIPTION

We consider a precoding-enabled geostationary earth orbit (GEO) satellite system consisting of a GW, a transponder capable of generating N beams, and $K (K \leq N)$ single-antenna UTs as shown in Fig. 2. The precoded signals transmitted from the satellite towards the UTs can be grouped in a vector $\mathbf{x} = [x_1, \ldots, x_N]$ related to the received signals at the UTs $\mathbf{r} = [r_1, \ldots, r_K]$ by

$$\mathbf{r} = \mathbf{H}\mathbf{x} + \mathbf{z}, \tag{1}$$

where $\mathbf{H}$ represents the $K \times N$ channel matrix and $\mathbf{z}$ contains the independent additive white Gaussian noise (AWGN) at the UTs modeled as circularly symmetric complex Gaussian random variables with zero mean and variance σ^2.

The channel matrix elements are complex-valued and are denoted as $|h_{k_n}|e^{j\psi_{k_n}}$, with $|h_{k_n}|$ represents the attenuation and ψ_{k_n} being the phase distortions to the beam n received by the k-th UT. To apply precoding technique, the intended modulated symbols $\mathbf{s} = [s_1, \ldots, s_K]$ are multiplied by the $N \times K$

precoding matrix $\mathbf{W}$, ($\mathbf{HW} = \mathbf{I}$) in such a way that (1) becomes

$$\mathbf{r} = \mathbf{HWs} + \mathbf{z} = \mathbf{s} + \mathbf{z}. \tag{2}$$

As such, the precoding matrix is calculated at the GW using the CSI from each UT. The CSI contains the channel estimation for each beam the k-th UT receives. Formally, it can be represented as $\hat{\mathbf{h}}_k = [\hat{h}_{k_1}, \ldots, \hat{h}_{k_N}]$, where $\hat{h}_{k_n}$ is the estimated complex channel coefficient. The CSI estimation[1] is performed at the UT using the non-precoded pilots periodically sent by the GW.

Other channel impairments could impact the precoding performance, but only those introducing time-varying phase differences across the beams [30]. For the presented scenario, these are the phase noise introduced by the local oscillator in the multi-beam payload [31] and the Doppler shifts for the different uplink subcarriers caused by the (although small) oscillatory relative movement of the GEO satellite with respect to the gateway [32]. Nevertheless, we assume the system implements the mitigation techniques proposed and demonstrated for such impairments [31], [32]. Therefore, these effects will be neglected in our analysis and experiments.

III. PRECODING IMPLEMENTATION

The DVB-S2X data streams are jointly precoded via the precoding block, which applies the precoding matrix $\mathbf{W}$ to the data symbols. According to [3], only certain fields of the DVB-S2X SF are precoded. For example, the precoding block is not activated at the start of SF (SOSF) and SF pilots. The SOSF is a known Walsh-Hadamard sequence that can be reliably detected at UTs even in high-interference conditions. On the other hand, the P-pilots are not precoded since they are used by the UTs to estimate the CSI, denoted by $\hat{\mathbf{H}}$, and to calculate the differential frequency and phase offset between the two spot beams. Note that the estimated CSI $\hat{\mathbf{H}}$ at the UTs is fed back through the return link and is repeatedly used to compute the precoding matrix coefficients by the GW. Optimal linear precoding relies heavily on precise knowledge of the CSI at the transmitter. However, in practical scenarios—especially in satellite communication where delay and Doppler effects can introduce additional complexity—obtaining accurate CSI can be challenging. Imperfections in CSI can lead to a mismatch between the actual and estimated channel conditions, resulting in suboptimal performance, such as residual interference and degraded signal quality. This sensitivity to CSI is particularly relevant in satellite systems, where the propagation delay and the mobility of ground terminals can further degrade the accuracy of CSI, making the implementation of optimal precoding more challenging compared to terrestrial systems. Therefore, it is crucial to feed back the estimated CSI from the UT via the return link to maintain effective precoding.

[1]This operation is supported by the DVB-S2X standard that establishes the alternate transmission of precoded data and non-precoded pilots in its superframe (SF) format structure. Considering standard DVB-S2X SF-compliant terminals helps in estimating the real-time CSI to facilitate precoding at the GW. Thus, the GW can compensate for the differential frequency and phase distortions introduced by the conventional satellite transponder design, as discussed in our previous work [29].

A. CALCULATION

In our experiments, three precoding schemes are implemented at the GW, namely, two different types of MMSE precoding and optimal linear precoding. The simplest precoder implemented at the GW is the MMSE scheme in its basic form [4], which is given by

$$\mathbf{W}_{\text{MMSE}} = \hat{\mathbf{H}}^{\text{H}}(\hat{\mathbf{H}}\hat{\mathbf{H}}^{\text{H}} + \sigma^2\mathbf{I})^{-1}, \tag{3}$$

with σ^2 denoting the noise variance measured at the UT side. Another type of precoding implemented at the GW is the so-called MMSE per-antenna power-constrained (PAC) in which the precoding matrix is calculated as

$$\mathbf{W}_{\text{MMSE-PAC}} = \hat{\mathbf{H}}^{\text{H}}(\hat{\mathbf{H}}\hat{\mathbf{H}}^{\text{H}} + \mathbf{\Lambda})^{-1}, \tag{4}$$

where the regularization $\mathbf{\Lambda}$ is a real diagonal matrix consisting of the Lagrangian dual variables. The optimal regularization $\mathbf{\Lambda}$ must satisfy

$$\mathbf{\Lambda}\left(\text{diag}(\mathbf{W}\mathbf{W}^{\text{H}}) - \phi\mathbf{I}\right) = \mathbf{0}, \tag{5}$$

where ϕ is the available per-antenna transmit power. To find the optimal $\mathbf{\Lambda}$, we use a low-complexity iterative method as proposed in [5] with its convergence proof. Note that, assuming symbols with unit average power, the squared Euclidean norms of the rows and columns of the precoding matrix respectively correspond to the per-antenna and per-beam power levels. The MMSE-PAC technique is particularly of interest as it yields a precoding matrix with all rows and columns normalized to have a squared norm of ϕ. For example, by setting $\phi = 1$, both per-antenna and per-beam power levels in $\mathbf{W}_{\text{MMSE-PAC}}$ are normalized to one. Nevertheless, further normalization steps are needed which may affect the optimality of the precoder.

The third precoding scheme is implemented based on the technique presented in [6]. We refer to this scheme as optimal linear (OPTL) precoding. Let $\mathbf{h}_i$ and $\mathbf{w}_i$ respectively denote the channel and the precoding vectors for the i-th UT such that $\mathbf{H} = [\mathbf{h}_1, \mathbf{h}_2, \ldots, \mathbf{h}_K]^{\text{H}}$ and $\mathbf{W}_{\text{OPTL}} = [\mathbf{w}_1, \mathbf{w}_2, \ldots, \mathbf{w}_K]$. The OPTL technique aims to find the optimum precoding vectors by solving the following virtual uplink problem as follows:

$$\begin{aligned} \min_{\mathbf{u}_i, p_i} \quad & \sum_{i=1}^{K} p_i \\ \text{s.t.} \quad & \frac{p_i \mathbf{u}_i^{\text{H}} \mathbf{h}_i \mathbf{h}_i^{\text{H}} \mathbf{u}_i}{\sum_{j \neq i} p_j \gamma_j \mathbf{u}_i^{\text{H}} \mathbf{h}_j \mathbf{h}_j^{\text{H}} \mathbf{u}_i + 1} \geq 1, \quad i = 1, 2, \ldots, K \\ & \|\mathbf{u}_i\|^2 = 1, \quad i = 1, 2, \ldots, K, \end{aligned} \tag{6}$$

where γ_j is the given signal-to-noise-and-interference ratio (SNIR) requirement for the j-th UT. The optimal precoding vectors are then obtained as $\mathbf{h}_i = \sqrt{p_i}\mathbf{u}_i$, for all $i \in$

$\{1, 2, \ldots, K\}$. To solve the problem in (6), an iterative algorithm is presented in [6] which is composed of two main steps, namely, beamformer update and power control update. The corresponding algorithm is summarized as in Algorithm 1, wherein the superscript t refers to the iteration number, with Q being the total number of iterations.

B. COMPLEXITY ANALYSIS

The complexity of designing precoding in (4) has two fold: (i) calculating $\mathbf{W}$; and (ii) computing Algorithm 1, which yields $\mathbf{\Lambda}$. In this context, the concrete takeaway messages of designing precoding in (4) are as follows:

- In both (i) and (ii), only linear vector and matrix calculation operations are required, leading to low complex designing of precoding $\mathbf{W}$.
- To calculate $\mathbf{\Lambda}$ via using Algorithm 1 in (ii), it is not necessary to consider greedy iterative search so that the number of Q is small. This will be justified later in analyzing the numerical results.

In the following, we resume the main operations needed to determine the precoding matrix using the proposed technique.
(i) Matrix summation or differentiation - $\mathcal{O}(K^0)$

(ii) Matrix multiplication for $K \times K$ matrices $\mathbf{A}$ and $\mathbf{B}$ - $\mathcal{O}(K^3)$

(iii) Matrix inversion - $\mathcal{O}(K^3)$

(iv) Multiplication and division of two vectors a and b - $\mathcal{O}(K)$

(v) Scalar multiplied with vector or matrix - $\mathcal{O}(K^0)$.

The rest of the operation complexities can be neglected. Assuming N_{iter} iterations and L_{frame} the length of the frame to which a single precoder is applied, the following complexity can be found:

- The complexity of calculating $\mathbf{W}$: $\mathcal{O}(3K^3)$ (over bundle frames)
- Complexity of calculating $\mathbf{\Lambda}$ into $\mathbf{W}$: $\mathcal{O}(6K^2 N_{\text{iter}})$ (over bundle frames)
- Complexity of application of precoding matrix $\mathbf{W}$: $\mathcal{O}(K^2)$ (per symbol)

It is clear that the application of the precoders (both standard MMSE or the proposed one), taking into account a system of 16 beams, counts more than the computation itself since the ratio between the symbol rate and the Bundle rate is about 67920 for Format 2 and about 16984 for Format 3. The above analysis does not take into account operations that are or are not parallelizable within an FPGA. This complexity analysis is crucial to justify the exclusion of optimization-based techniques. According to the literature, the complexity of each iteration for solvers such as the interior point method used to solve Semi-Definite Programming problems in CVX is $\mathcal{O}(K^6)$ [33]. Although low-complexity methods or optimized techniques could potentially reduce this complexity, their performance has not been validated in satellite systems.

Algorithm 1: OPTL Precoding.

input : $\{\mathbf{h}_i, \gamma_i\}_{i=1}^K$
output : $\{\mathbf{w}_i\}_{i=1}^K$
$t = 0,\ p_i^{(0)} = 1,\ i = 1, 2, \ldots, K$
while *the terminating condition is not met* **do**
Beamformer update:
$\mu_i^{(t+1)} \leftarrow \max_{\|\mathbf{u}_i\|=1} \frac{p_i{}^{(t)} \mathbf{u}_i^{\mathrm{H}} \mathbf{h}_i \mathbf{h}_i^{\mathrm{H}} \mathbf{u}_i}{\sum_{j \neq i} p_j{}^{(t)} \gamma_j \mathbf{u}_i^{\mathrm{H}} \mathbf{h}_j \mathbf{h}_j^{\mathrm{H}} \mathbf{u}_i + 1}$
Power control update:
$p_i^{(t+1)} \leftarrow (\gamma_i / \mu_i)\, p_i^{(t)}$
$t \leftarrow t + 1$
end while
$\mathbf{q} = [\gamma_1 \sigma^2, \gamma_2 \sigma^2, \ldots, \gamma_K \sigma^2]^{\mathrm{T}}$
$[\mathbf{F}]_{i,j} = \begin{cases} \mathbf{u}_i^{\mathrm{H}} \mathbf{h}_i \mathbf{h}_i^{\mathrm{H}} \mathbf{u}_i, & i = j, \\ -\gamma_i \mathbf{u}_j^{\mathrm{H}} \mathbf{h}_j \mathbf{h}_j^{\mathrm{H}} \mathbf{u}_j, & i \neq j \end{cases}$
$\mathbf{p} = \mathbf{F}^{-1} \mathbf{q}$
$\mathbf{w}_i = \sqrt{[\mathbf{p}]_i}\, \mathbf{u}_i$.

C. NORMALIZATION

To address the requirements of the GW feeder link, we have to ensure a unit output signal power for each transmit antenna. From the optimization problem in (6), it follows that the OPTL design satisfies the sum power constraint but has no control over the per-antenna powers. Therefore, our implementation of the OPTL precoding includes an additional row-wise normalization so that each row of the precoding matrix $\mathbf{W}_{\text{OPTL}}$ has a unit Euclidean norm.

IV. EXPERIMENTAL VALIDATION

The experimental validation corresponding to the 16×16 AWGN channel emulation is depicted in this section. For the satellite link, we emulated the SES-14 satellite. The beam patterns, HPA, and thermal noise were simulated to emulate the SES-14 satellite link. SES-14 is operational since 2018. The hybrid satellite provides C-and Ku-band wide beam coverage, as well as Ku-and Ka-band HTS coverage across the Americas and the North Atlantic region. Also, SES-14 has two spot beams in the Ku-band covering a part of Western Europe and the United Kingdom. We show the approximated spot beams in Fig. 3. The In-Lab equipment setup and overview are shown in Fig. 4 and Fig. 5, respectively. The in-house developed MIMO end-to-end satellite emulator includes several key components: a multichannel GW with precoding functionality, a MIMO satellite channel emulator (ChEm), multiple independent UTs, and a return-link emulator.

To summarize the system: the GW subsystem is responsible for producing data packets following the DVB-S2X standard, utilizing the SF format II structure, and implementing the chosen precoding technique. The ChEm replicates the whole forward link chain, from the intermediate frequency (IF) input

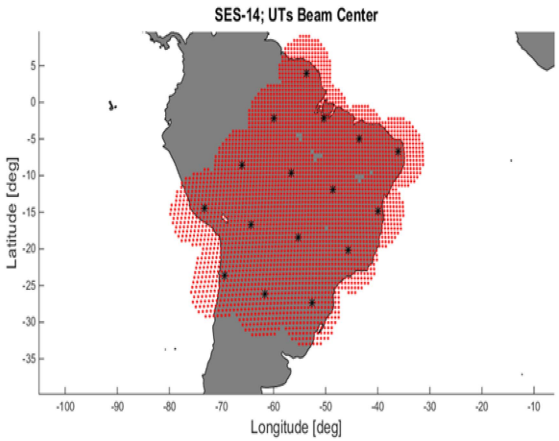

FIGURE 3. SES-14 scenario SES14_A1, 16 Beams over South America, users at beam center.

FIGURE 4. In-Lab demo equipment.

of the GW block up-converter (BUC), toward the low-noise block down-converter (LNB) IF output at the user terminal. It emulates the impairments present in the GW, the payload, the downlink channel, and the UTs. The UTs implement the synchronization and decoding features in the DVB-S2X-compliant receivers and perform the CSI estimation. Finally, the return-link emulator allows each UT to send its estimated CSI to the GW. Additional details on the demonstrator subsystems can be found in [29]. The current implementation is an upgraded version of the setup presented in the cited work, extending the MIMO emulation capabilities from 6×6 to 16×16 channels. It is also worth noting that the developed

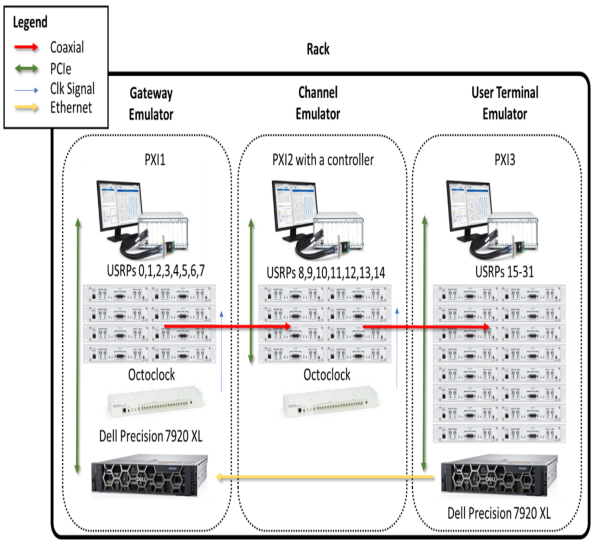

FIGURE 5. In-Lab demo setup overview.

TABLE 1. Summary of the Hardware Components of the In-Lab Demo

Item	Number/Subsystem		
	GW	UTs	ChEm
USRP RIO 2945R	8	16	8
PXIe-1085	1	1	1
FlexRIO field programmable gate array (FPGA)	1	0	1
Octoclock	1 (common)		
Embedded controller for PXIe-1085	0	0	1
Computer servers	1	1	0

TABLE 2. Lab Demo Computers Specifications

Feature	Server Computer	Embedded Controller
Model	Dell Precision 7920 XL	NI PXIe-8153
CPU	Intel Xeon Gold 6148	Intel Core i7-3610QE
RAM	48 GB	16 GB
Storage	1 TB SSD	512 GB SSD
OS	Microsoft Windows 10 (64 bits)	Microsoft Windows 7 (64 bits)
Development SW	NI LabVIEW NXG 3.1	

DVB-S2X modems performance has been successfully tested over a live GEO link [26].

The hardware components associated with the In-Lab demo are summarized in Table 1, with the specifications for computers controlling the SDR platforms given in Table 2. Additionally, each server is equipped with a peripheral component interconnect express (PCIe)-8381 host interface card to control the NI peripheral component interconnect (PCI) extensions for instrumentation (PXI) chasses from the servers. A PXI remote control module is placed in the system slot of the PXI chassis and a host interface card is used in the host server. This allows the host computer to establish a PCI Express connection to the chassis using a compatible multisystem extension interface (MXI)-Express cable and simultaneously operate all the universal software radio peripherals (USRPs).

TABLE 3. System Parameter Used for the Experiments

Parameter	Value
Orbit	GEO, 47.5 deg west
Coverage	16 beams over South America
No. of active beams	16
Transponder BW	54 MHz
Symbol rate	20 MSPS
Roll-off factor	0.2
Symbol Rate	20 MSPS
Carrier frequency	11.73 GHz
Air interface	DVB-S2X, SuperFraming
No. of carriers per transponder	1
Adaptive coding and modulation (ACM) margin	0.6 dB
Oversampling factor	4

We performed hardware-in-loop (HIL) testing with real-time channel emulation providing a close approximation of practical conditions, making our results applicable to real-world scenarios. The performance of the In-Lab test is evaluated for different frequency reuse configurations using MMSE precoder with PAC, MMSE precoder with maximum power constraint (MPC), and 4FR. These comparisons for frequency allocation techniques are made with respect to three conditions of CSI. The first CSI condition is that precoders are calculated considering the ideal channel matrix, whereas the second and third CSI conditions are based on the calculation of precoders with CSI errors corresponding to the normal CSI and ESA NGW project. The parameters used for all experiments are summarized in Table 3.

V. RESULTS AND DISCUSSION

In this section, the performance of the precoders is evaluated with respect to the received precoded SNIR amongst beams versus the per-beam peak power. The results are as a function of the satellite per antenna power (P_{sat}) minus the output back-Off (OBO). It is noteworthy that the FFR configurations use half of the power of the 4FR since the throughput is calculated on the per-polarization SNIR and then multiplied by a factor of two (both polarizations). Specifically, with PAC we refer to the per-line normalization of the precoding matrix so that the transmission power is maximized for each antenna, whereas with MPC we refer to the power scaling applied to the whole precoder based on the maximum value calculated on per-line in the precoding matrix. In order to account for the channel amplifier (CAMP) effect, and in particular, for the normalization effect of the automatic level control (ALC) which normalizes over the signal power, a per-line re-scaling of the precoder is performed and termed as per-antenna power re-scaling (PAR). Hereby, a fair comparison of MMSE-PAC is performed with the MMSE.

From Figs. 6 and 7, it can be visualized that for the operational point, which is 4.5 dBW, MMSE-PAC has better performance in terms of SNIR and total throughput as compared to MMSE. The average SNIR for MMSE-PAC at 4.5 dBW is 6.8 dB for estimated and actual ones, whereas, for MMSE-PAR, it is around 5.9 dB for estimated and actual.

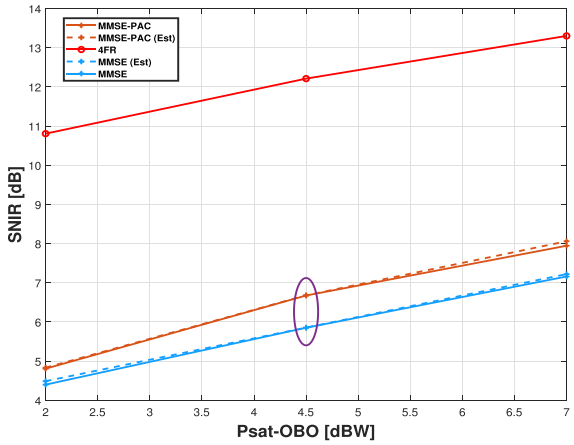

FIGURE 6. Numerical results for SES-14 scenario SES14_A1 and performance comparison between obtained average SNIR and Psat using CSI errors.

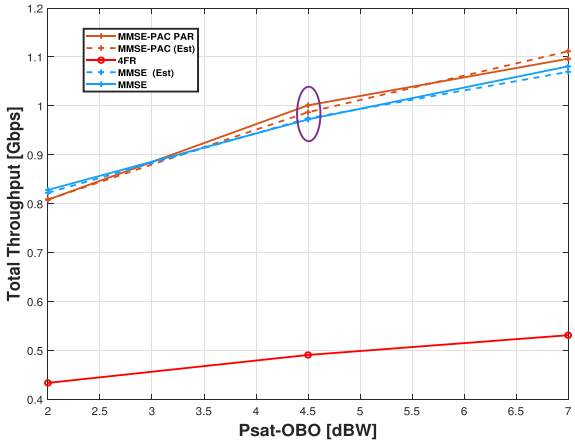

FIGURE 7. Numerical results for SES-14 scenario SES14_A1 and performance comparison between obtained total throughput and Psat using CSI errors.

While throughput increased from 0.96 Gbps to 1 Gbps using the MMSE-PAC if compared with the MMSE.

It is worth noting that both precoding schemes show lower SNIR than the 4FR technique. However, this is an expected result, as the conservative 4FR allocation has been conceived to minimize the interference by spacing the beams that use the same carrier frequency but at the price of using less bandwidth. The advantage of precoding is observed in a significant throughput increase regardless of the lower SINR, as depicted in Fig. 7, due to exploiting a larger bandwidth. This can be understood considering the throughput is proportional to the product of spectral efficiency and the bandwidth, with the spectral efficiency being dependent on the MODCOD (modulation and coding) selected as a function of the SINR. While the spectral efficiency when using precoding is lower than the 4FR transmission, the higher throughput comes from improving the frequency spectrum usage (full bandwidth, i.e., four times larger bandwidth than in 4FR).

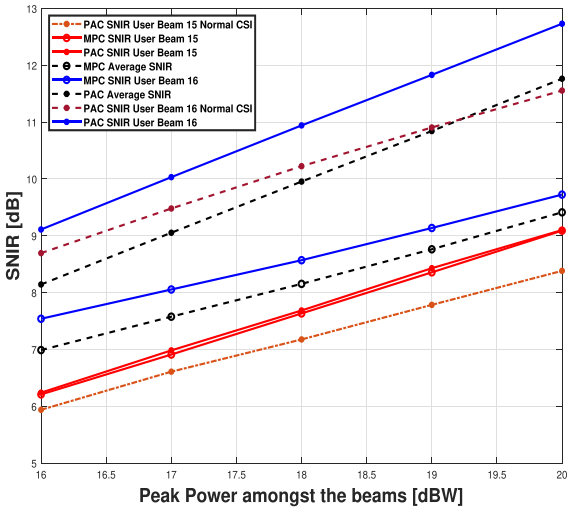

FIGURE 8. Obtained SNIR for beams 16 and 15 as a function of Psat using CSI errors.

While Fig. 6 aims at evaluating the average received SNIR performance over the whole coverage, in Fig. 8 the objective is to highlight the received SNIR performance versus (P_{sat}) by focusing on some specific users in some specific beams. The received SNIR performance is more sensitive to errors in the estimation (mainly nullification) for higher power transmissions. To highlight this aspect, the curve for PAC SNIR User Beam 16 has to be compared with the curve for PAC SNIR User Beam 16 Normal CSI, and the curve for PAC SNIR User Beam 15 has to be compared with the curve for PAC SNIR User Beam 15 Normal CSI.

Finally, based on Scenario SES14$_A$1 as illuminated earlier in Fig. 3, 16 $\times$ 16 scenario has been tested with the In-Lab demo with all the users located in the beam centers. Accordingly, in the case of MMSE precoding, we used two different power constraints: in the first case, we rely on the constant power spectral density (PSD) assumption between the FFR and 4FR systems, whereas in the second case, we rely on a constant total power constraint. In particular, we use as a reference the power of the precoding case, so the PSD of the precoding is not changing, while the PSD of the 4FR in this configuration increases, leading to an increase of the SNIR in the 4FR constant total power scenario. For the MMSE-PAC precoding technique, only the constant PSD power constraint has been tested. Corresponding to the above, the results are summarized from Table 4 to Table 7, whereby one can note the significant advantages brought by the MMSE-PAC precoding technique in terms of average SNIR and system throughput.

TABLE 4. Scenario SES14$_A$1 MMSE SNIR Comparison (In Db)

UT	FFR (MMSE)	4FR (const. PSD)	4FR (const. total power)
UT1	11.77	15.96	20.45
UT2	12.99	17.23	21.42
UT3	12.54	15.56	19.85
UT4	12.14	16.49	20.75
UT5	13.61	17.06	21.59
UT6	14.95	17.58	22.08
UT7	12.16	15.22	19.87
UT8	12.46	16.58	21.07
UT9	13.57	14.67	19.24
UT10	12.73	15.55	19.78
UT11	11.95	15.65	20.05
UT12	12.21	15.41	19.61
UT13	13.61	16.43	20.87
UT14	13.34	16.04	20.18
UT15	12.14	15.70	19.64
UT16	10.51	15.00	19.28
Average	12.67	16.07	20.36

TABLE 5. Scenario SES14$_A$1 MMSE Precoding Throughput Comparison (In Mbps)

UT	FFR (MMSE)	4FR (const. PSD)	4FR (const. total power)
UT1	16.11	5.36	6.69
UT2	17.14	6.01	6.69
UT3	17.14	5.36	6.69
UT4	16.11	5.36	6.69
UT5	17.14	6.01	6.69
UT6	21.45	6.01	6.69
UT7	16.11	5.36	6.69
UT8	16.11	5.36	6.69
UT9	17.14	5.36	6.69
UT10	17.14	5.36	6.69
UT11	16.11	5.36	6.69
UT12	16.11	5.36	6.69
UT13	17.14	5.36	6.69
UT14	17.14	5.36	6.69
UT15	16.11	5.36	6.69
UT16	14.48	5.36	6.69
System	268.70	87.77	107.10

VI. CONCLUSION

In this work, we implemented optimal linear precoders at the GW for multibeam GEO satellite systems to mitigate the issue of multi-user interference. We demonstrated the use of standard DVB-S2X SF-compliant terminals capable of estimating real-time CSI to facilitate effective precoding at the GW. Using the SF structure, the GW can compensate for the differential frequency and phase distortions introduced by conventional satellite transponder designs. Field tests confirmed the end-to-end SNIR and coded throughput gains achievable through precoded communications over the actual satellite forward link. The results demonstrated that terminal-specific data could be reliably transmitted to independent UTs through the same physical channel by leveraging closed-loop precoding over a multi-beam satellite. Furthermore, we showed that precoding techniques, when combined with FFR, significantly outperform conventional 4FR schemes. Performance evaluations revealed that the MMSE-PAC scheme outperforms MMSE-PAR in terms of SNIR and throughput at the 4.5 dBW operational point.

TABLE 6. Scenario SES14$_A$1 MMSE-PAC SNIR Comparison (In Db)

UT	FFR (MMSE-PAC)	4FR (const. PSD)
UT1	10.95	15.96
UT2	13.20	17.23
UT3	12.10	15.56
UT4	11.72	16.49
UT5	12.85	17.06
UT6	15.18	17.58
UT7	11.35	15.22
UT8	11.86	16.58
UT9	16.11	14.67
UT10	17.14	15.55
UT11	17.14	15.65
UT12	16.11	15.41
UT13	17.14	16.43
UT14	21.45	16.04
UT15	16.11	15.70
UT16	16.11	15.00
Average	14.78	16.07

TABLE 7. Scenario SES14$_A$1 MMSEPAC Throughput (In Mbps)

UT	FFR (MMSE-PAC)	4FR (const. PSD)
UT1	17.9696	6.7122
UT2	26.8489	6.7122
UT3	17.9696	6.7122
UT4	17.9696	6.7122
UT5	26.8489	6.7122
UT6	26.8489	6.7122
UT7	17.9696	6.7122
UT8	17.9696	6.7122
UT9	17.14	5.36
UT10	17.14	6.01
UT11	16.11	5.36
UT12	16.11	5.36
UT13	17.14	5.36
UT14	17.11	5.36
UT15	16.11	5.36
UT16	14.48	5.36
System	301.72	97.22

However, a critical challenge identified is the sensitivity of optimal linear precoding to inaccuracies in CSI, especially at higher power transmission levels. Optimal linear precoding relies heavily on precise knowledge of the CSI at the transmitter. In practical scenarios—particularly in satellite communication where delays and Doppler effects introduce additional complexity—obtaining accurate CSI can be challenging. Imperfections in CSI can lead to a mismatch between the actual and estimated channel conditions, resulting in suboptimal performance, such as residual interference and degraded signal quality. This challenge is especially pronounced in satellite systems, where the propagation delay and mobility of ground terminals can further degrade CSI accuracy, making the implementation of optimal precoding more difficult compared to terrestrial systems. Therefore, it is crucial to continuously feed back the estimated CSI from the UT via the return link to maintain effective precoding. Overall, our analysis highlights that while optimal linear precoding offers significant gains in data transmission efficiency, its success depends on accurate CSI estimation and feedback. This advancement not only enhances data transmission efficiency but also paves the way for more robust and adaptable satellite communication systems, showcasing the potential for future applications in various satellite communication scenarios.

VI. APPENDIX: CSI ESTIMATION ACCURACY

In this section, we evaluate the CSI accuracy performance over the 16x16 satellite demo. For this purpose, we use the following measure

$$\mathbf{G}(n) = \mathbf{H}_{est}(n) \times \mathbf{H}_{act}^{-1}, \tag{7}$$

where $\mathbf{H}_{est}(n)$ denotes the estimated CSI reported by the UTs at time instant n and $\mathbf{H}_{act}$ is the actual channel matrix loaded into the channel emulator. Both $\mathbf{H}_{est}$ and $\mathbf{H}_{act}$ are 16×16 matrices where each row collects the channel coefficients for a UT over different beams. The diagonal and the off-diagonal elements of $\mathbf{G}(n)$ respectively correspond to the desired signal and the interference from the adjacent beams. If the channel estimation is perfect, $\mathbf{G}(n)$ is a diagonal matrix up to a scaling factor. However, this is not the case in practice due to the imperfect channel estimation process and the UT's receiver noise. In the sequel, we plot the element-wise mean (E) and variance var of $\mathbf{G}(n)$ calculated over N realizations, respectively, as follows:

$$E\left[\mathbf{G}(n)\right] = \frac{1}{N}\sum_{n=1}^{N}\mathbf{G}(n) \tag{8}$$

$$var\left[\mathbf{G}(n)\right] = \frac{1}{N}\sum_{n=1}^{N}\{(\mathbf{G}(n) - E\left[\mathbf{G}(n)\right]) \circ (\mathbf{G}(n) - E\left[\mathbf{G}(n)\right])^*\} \tag{9}$$

with $\circ$ denoting the element-wise product.

For this test, we consider two realizations for the channel with different interference conditions. Namely, we assume the off-diagonal channel coefficients to be 0.05 or 0.1 times smaller than the diagonal coefficients. The two considered channels are as follows:

$$\mathbf{H}_{act}^{5\%} = \begin{bmatrix} 0.5 & \dots & 0.025 \\ \vdots & \ddots & \vdots \\ 0.025 & \dots & 0.5 \end{bmatrix},$$

$$\mathbf{H}_{act}^{10\%} = \begin{bmatrix} 0.5 & \dots & 0.05 \\ \vdots & \ddots & \vdots \\ 0.05 & \dots & 0.5 \end{bmatrix} \tag{10}$$

Moreover, we introduced a noise power at each UT equivalent to a signal-to-noise ratio (SNR), i.e., with respect to the main beam without interference, of 16 dB. Fig. 9 and Fig. 10 depicts the $\mathbf{G}(n)$ statistics results obtained over $N = 100$ realizations.

The accuracy of the CSI estimation in the experimental setup can be observed in the likelihood of the measured mean values (subfigures a) with diagonal matrices, as expected results from ideal estimations. The results show the off-diagonal elements of $\mathbf{G}(n)$ being more than 20 dB below the diagonal elements level, denoting a highly accurate estimation.

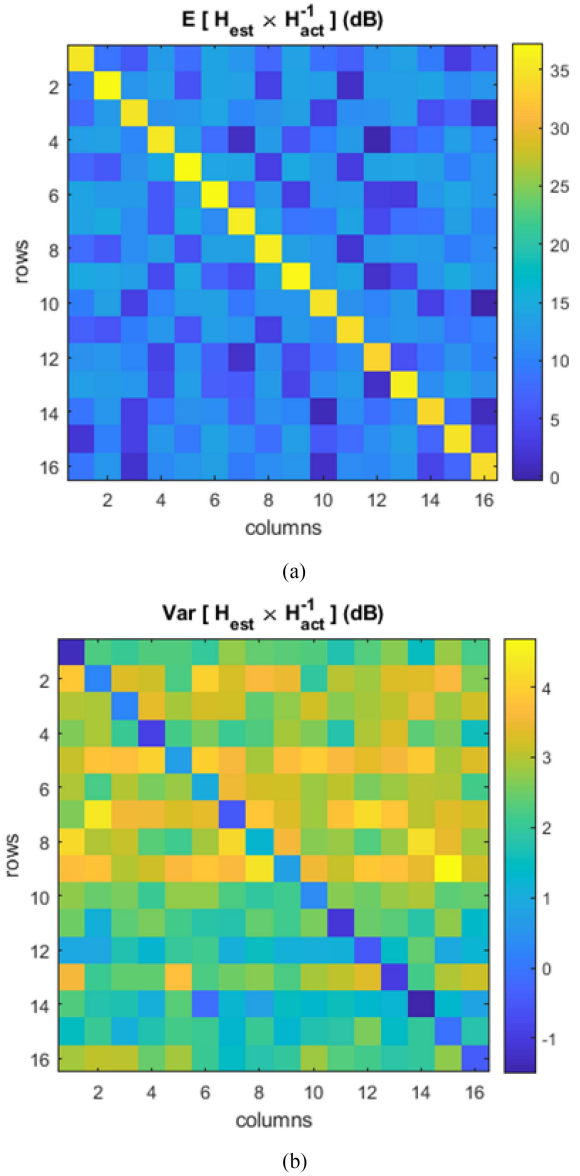

FIGURE 9. Results with $\mathbf{H}_{act}^{5\%}$: (a) element-wise mean, and (b) element-wise variance.

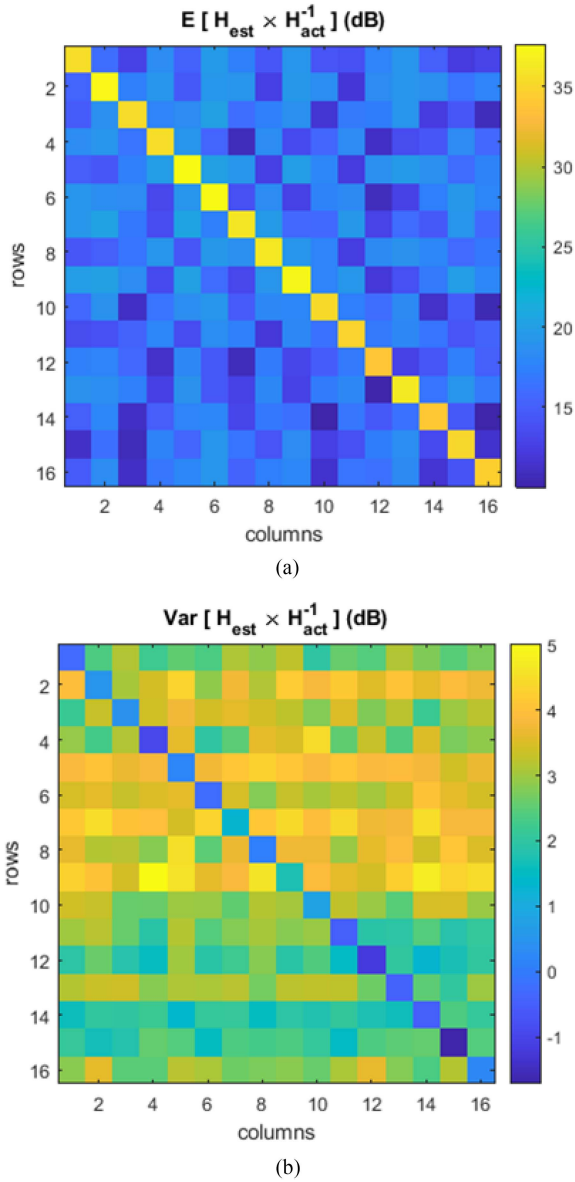

FIGURE 10. Results with $\mathbf{H}_{act}^{10\%}$: (a) element-wise mean, and (b) element-wise variance.

ACKNOWLEDGMENT

"Live Satellite Demonstration of Advanced Interference Management Techniques (LiveSatPreDem)" and SES S.A. (Opinions, interpretations, recommendations, and conclusions presented in this paper are those of the authors and are not necessarily endorsed by the European Space Agency or SES).

REFERENCES

[1] D. Minoli, *Innovations in Satellite Communications and Satellite Technology: The Industry Implications of DVB-S2X, High Throughput Satellites, Ultra HD, M2M, and IP*. Hoboken, NJ, USA: Wiley, 2015.

[2] V. Joroughi, S. M. Bhavani, S. Maleki, S. Chatzinotas, J. Grotz, and B. Ottersten, "Robust precoding and beamforming in a multiple gateway multibeam satellite system," in *Proc. IEEE Glob. Commun. Conf.*, 2018, pp. 1–7.

[3] ETSI TS 102 376-2, "Digital Video Broadcasting (DVB); Implementation Guidelines for the Second Generation System for Broadcasting, Interactive Services, News Gathering and Other Broadband Satellite Applications; Part 2: S2 Extensions (DVB-S2X)," 2021.

[4] C. B. Peel, B. M. Hochwald, and A. L. Swindlehurst, "A vector-perturbation technique for near-capacity multiantenna multiuser communication part i: Channel inversion and regularization," *IEEE Trans. Commun.*, vol. 53, no. 1, pp. 195–202, Jan. 2005.

[5] H. Shen, B. Li, M. Tao, and X. Wang, "MSE-Based transceiver designs for the MIMO interference channel," *IEEE Trans. Wireless Commun.*, vol. 9, no. 11, pp. 3480–3489, Nov. 2010.

[6] M. Bengtsson and B. Ottersten, "Optimal and suboptimal transmit beamforming," in *Handbook Antennas in Wireless Commun.*. Boca Raton, FL, USA: CRC Press, 2001.

[7] A. Morello and V. Mignone, "DVB-S2X: The new extensions to the second generation DVB satellite standard DVB-S2," in *Int. J. Satellite Commun. Netw.*, vol. 34, pp. 323–325, 2016.

[8] L. M. Marrero, J. C. M. Duncan, J. Querol, S. Chatzinotas, A. J. C. Carmona, and B. Ottersten, "Effects of differential oscillator phase noise in precoding performance," in *Proc. IEEE Adv. Commun. Satell. Syst.. Proc. 37th Int. Commun. Satell. Syst. Conf.*, 2019, pp. 1–15.

[9] A. Haqiqatnejad, F. Kayhan, and B. Ottersten, "Robust design of power minimizing symbol-level precoder under channel uncertainty," in *Proc. IEEE Glob. Commun. Conf.*, 2018, pp. 1–6.

[10] N. Maturo et al., "Demonstrator of precoding technique for a multi-beams satellite system," in *Proc. IEEE 8th Int. Workshop Tracking, Telemetry Command Syst. Space Appl.*, 2019, pp. 1–8.

[11] A. Tato, S. Andrenacci, S. Chatzinotas, and C. Mosquera, "Link adaptation and carriers detection errors in multibeam satellite systems with linear precoding," in *Proc. IEEE 9th Adv. Satell. Multimedia Syst. Conf. 15th Signal Process. Space Commun. Workshop*, 2018, pp. 1–8.

[12] B. Clerckx and C. Oestges, *MIMO Wireless Networks: Channels, Techniques and Standards for Multi-Antenna, Multi-User and Multi-Cell Systems*. New York, NY, USA: Academic Press, 2013.

[13] J. Krivochiza, J. M. Duncan, S. Andrenacci, S. Chatzinotas, and B. Ottersten, "FPGA acceleration for computationally efficient symbol-level precoding in multi-user multi-antenna communication systems," *IEEE Access*, vol. 7, pp. 15509–15520, 2019.

[14] N. Mazzali, S. Boumard, J. Kinnunen, B. S. MR, M. Kiviranta, and N. Alagha, "Enhancing mobile services with DVB-S2X superframing," *Int. J. Satell. Commun. Netw.*, vol. 36, no. 6, pp. 503–527, 2018.

[15] S. Jiang, F.-K. Gong, and X. Chen, "A low-complexity soft demapper for 128APSK of DVB-S2X," in *Proc. IEEE 8th Int. Conf. Wireless Commun. Signal Process.*, 2016, pp. 1–4.

[16] J.-A. Lucciardi, P. Potier, G. Buscarlet, F. Barrami, and G. Mesnager, "Non-linearized amplifier and advanced mitigation techniques: DVB-S2X spectral efficiency improvement," in *Proc. IEEE Glob. Commun. Conf.*, 2017, pp. 1–7.

[17] M. A. Vazquez et al., "Precoding in multibeam satellite communications: Present and future challenges," *IEEE Wireless Commun.*, vol. 23, no. 6, pp. 88–95, Dec. 2016.

[18] V. Joroughi, M. Ã. Vazquez, and A. I. Perez-Neira, "Generalized multicast multibeam precoding for satellite communications," *IEEE Trans. Wireless Commun.*, vol. 16, no. 2, pp. 952–966, Feb. 2017.

[19] E. Lagunas, A. Pérez-Neira, M. Martínez, M. A. Lagunas, M. A. Vázquez, and B. Ottersten, "Precoding with received-interference power control for multibeam satellite communication systems," *Front. Space Technol.*, vol. 2, pp. 1–12, 2021.

[20] J. Duncan, J. Krivochiza, S. Andrenacci, S. Chatzinotas, and B. Ottersten, "Hardware demonstration of precoded communications in multi-beam UHTS systems," in *Proc. IEEE 36th Int. Commun. Satell. Syst. Conf.*, 2018, pp. 1–5.

[21] J. Krivochiza, J. C. Merlano-Duncan, S. Andrenacci, S. Chatzinotas, and B. Ottersten, "Computationally and energy efficient symbol-level precoding communications demonstrator," *Phys. Commun.*, vol. 28, pp. 108–115, 2018.

[22] J. C. Merlano-Duncan, J. Krivochiza, S. Andrenacci, S. Chatzinotas, and B. Ottersten, "Computationally efficient symbol-level precoding communications demonstrator," in *Proc. IEEE 28th Annu. Int. Symp. Pers., Indoor, Mobile Radio Commun.*, 2017, pp. 1–5.

[23] S. Chatzinotas, B. Ottersten, and R. De Gaudenzi, *Cooperative and Cognitive Satellite Systems*. New York, NY, USA: Academic Press, 2015.

[24] D. Spano, M. Alodeh, S. Chatzinotas, and B. Ottersten, "Per-antenna power minimization in symbol-level precoding," in *Proc. IEEE Glob. Commun. Conf.*, 2016, pp. 1–6.

[25] D. Spano, M. Alodeh, S. Chatzinotas, J. Krause, and B. Ottersten, "Spatial PAPR reduction in symbol-level precoding for the multi-beam satellite downlink," in *Proc. IEEE 18th Int. Workshop Signal Process. Adv. Wireless Commun.*, 2017, pp. 1–5.

[26] J. Krivochiza et al., "End-to-end precoding validation over a live GEO satellite forward link," in *IEEE Access*, vol. 11, pp. 41556–41564, 2021.

[27] V. M. Baeza, V. N. Ha, J. Querol, and S. Chatzinotas, "Non-coherent massive MIMO integration in satellite communication," in *Proc. IEEE 27th Ka 39th ICSSC Joint Conf.*, 2022, pp. 200–205.

[28] ETSI TS 102 376-1, "Digital Video Broadcasting (DVB); Implementation Guidelines for the Second Generation System for Broadcasting, Interactive Services, News Gathering and Other Broadband Satellite Applications; Part 1: DVB-S2," 2015.

[29] J. Duncan et al., "Hardware precoding demonstration in multi-beam UHTS communications under realistic payload characteristics," in *Proc. IEEE Adv. Commun. Satell. Syst.. 37th Int. Commun. Satell. Syst. Conf.*, 2019.

[30] L. M. Marrero, A. Haqiqatnejad, J. C. M. Duncan, S. Chatzinotas, and B. Ottersten, "Multiuser-MISO precoding under channel phase uncertainty in satellite communication systems," *IEEE Open J. Veh. Technol.*, vol. 4, pp. 127–148, 2023.

[31] L. M. Marrero et al., "Accurate phase synchronization for precoding-enabled GEO multibeam satellite systems," *IEEE Open J. Commun. Soc.*, vol. 5, pp. 712–729, 2024.

[32] J. L. González-Rios et al., "Doppler shift in precoded cooperative multi-gateway satellite systems: Effects and mitigation," in *Proc. IEEE Wireless Commun. Netw. Conf.*, 2024, pp. 1–6.

[33] D. Christopoulos, S. Chatzinotas, and B. Ottersten, "Weighted fair multicast multigroup beamforming under per-antenna power constraints," *IEEE Trans. Signal Process.*, vol. 62, no. 19, pp. 5132–5142, Oct. 2014.